Chemical Science

ROYAL SOCIETY OF CHEMISTRY

EDGE ARTICLE

View Article Online
View Journal | View Issue

Open Access Article. Published on 20 August 2025. Downloaded on 11/7/2025 7:42:28 PM.
This article is licensed under a Creative Commons Attribution-NonCommercial 3.0 Unported Licence.

Check for updates

Cite this: *Chem. Sci.*, 2025, **16**, 16780

All publication charges for this article have been paid for by the Royal Society of Chemistry

# Detecting ALDH2 activity in live cells *via* conditional metabolic labeling

Weisong Lv,†[ab] Zheng Wang,†[ab] Can Zhang,[b] Taorui Yang,[a] Tao Liu,[b] Jia Li,[ab] Xiaohui Fan *[ab] and Xin Li *[ab]

Detecting enzyme activity that catalyzes subtle functional group transformations in live cells remains a major challenge. We introduce a conditional metabolic labeling strategy for enzymatic activity detection (cMLEAD), which harnesses cellular metabolic pathways to deliver indirect yet reliable activity readouts. Unlike traditional metabolic labeling approaches relying on nonspecific incorporation of tagged biomolecules, cMLEAD employs a tagged precursor whose metabolic incorporation is strictly dependent on specific enzymatic activity, effectively transforming a metabolic labeling event into an enzyme-activity measurement. Using aldehyde dehydrogenase 2 (ALDH2) as a proof of concept, we demonstrate the robustness of the strategy. cMLEAD for ALDH2 employs azido-tagged acetaldehyde, metabolized by ALDH2 into azidoacetate, which feeds into the acetyl-CoA biosynthetic pathway and is incorporated into lysine acylation, enabling fluorescence-based detection *via* click chemistry. The assay reliably reports ALDH2 activity, as validated through genetic and pharmacological modulation. cMLEAD further revealed suppressed ALDH2 activity under cellular senescence and oxidative stress, with direct inhibition by $H_2O_2$ likely contributing in part. Notably, cMLEAD is complementary to conventional *in vitro* assays and advantageous in preserving the native enzyme context. Leveraging this advantage, we developed a screening platform that identified sennoside A as a candidate ALDH2 activator, which alleviated light-induced retinal degeneration in mice. This study establishes cMLEAD as a robust and versatile platform for probing ALDH2 activity in pathophysiologically relevant contexts and facilitating therapeutic discovery. We envision the conceptual framework of cMLEAD may be adapted to other enzymes whose catalytic products feed into detectable metabolic incorporation.

Received 9th June 2025
Accepted 8th August 2025

DOI: 10.1039/d5sc04198h

rsc.li/chemical-science

## Introduction

Enzymes are biological catalysts essential for facilitating biochemical reactions and regulating metabolic pathways. Cellular enzyme activity fluctuates dynamically, enabling cells to adapt to environmental changes. Detecting enzyme activity is critical for understanding cellular functions and the mechanisms underlying various diseases.[1] Traditional biochemical assays typically require cell lysis to release enzymes,[2] which can disrupt their native conformation and activity. Furthermore, isolating enzymes from their cellular context eliminates critical interactions that modulate function and loses real-time dynamic information.[3] Consequently, these methods may not accurately reflect *in vivo* enzyme behavior,[4] underscoring the need for innovative approaches that enable real-time monitoring within live cells.

Recent advancements have introduced activity-based small-molecule probes for measuring enzyme activity in live cells.[5–8] These probes typically consist of organic dyes conjugated to natural substrates, with activatable signals generated by enzyme-catalyzed cleavage reactions. For instance, fluorophore–peptide conjugates detect protease activity;[9] phosphorylated fluorophores monitor phosphatases;[10] and fluorophore–saccharide conjugates track glycosidases.[11] These enzymes generally tolerate significant structural changes in their substrates, and their cleavage-based reactions facilitate robust activatable signals. While these designs have yielded practical tools for detecting enzyme activities in intact cells, their efficacy diminishes when applied to enzymes that catalyze subtle chemical transformations, particularly those whose native substrates allow only minimal structural modification. The key challenges lie in maintaining efficient enzymatic turnover and in generating distinguishable fluorescence signals for reliable readouts.

Aldehyde dehydrogenase 2 (ALDH2) exemplifies this challenge. ALDH2 catalyzes the oxidation of aldehydes into carboxylic acids, with acetaldehyde as its primary substrate.[12] Impaired ALDH2 function leads to the accumulation of toxic aldehydes, which are associated with numerous health risks,

[a]College of Pharmaceutical Sciences, Zhejiang University, 866 Yuhangtang Street, Hangzhou 310058, China. E-mail: fanxh@zju.edu.cn; lixin81@zju.edu.cn

[b]State Key Laboratory of Chinese Medicine Modernization, Innovation Center of Yangtze River Delta, Zhejiang University, Jiashan 314100, China

† These authors contributed equally to this work.



© 2025 The Author(s). Published by the Royal Society of Chemistry

Open Access Article. Published on 20 August 2025. Downloaded on 11/7/2025 7:42:28 PM.
This article is licensed under a Creative Commons Attribution-NonCommercial 3.0 Unported Licence.

including alcohol-related disorders,[13] cardiovascular diseases,[14] neurodegenerative disorders,[15] and cancers.[16] Importantly, ALDH2 activation has shown therapeutic potential, offering protection against cardiac ischemia,[17] cognitive deficits in Alzheimer's models,[18] and septic acute respiratory distress syndrome.[19] While ALDH2 is implicated in these pathologies, the mechanisms regulating its activity under various stress conditions remain poorly understood. Reliable methods for monitoring ALDH2 activity are therefore critical for elucidating its biological functions, uncovering its regulatory mechanisms, and discovering potential ALDH2 activators with therapeutic implications. ALDH2 activity is typically assessed using a standard *in vitro* spectrophotometric assay that monitors the conversion of $NAD^+$ to NADH (Fig. 1A).[17] However, this approach lacks the native cellular context and does not capture its dynamic regulation in live cells. While aldehyde-based fluorescent probes have been successfully developed for some other ALDH isoforms (Fig. 1B),[20,21] designing selective probes for ALDH2 remains difficult, partly due to structural constraints. ALDH2's substrate-binding pocket is optimized for small-sized aldehydes and imposes steric limitations that restrict the incorporation of bulky fluorescent groups.[22–24]

Herein, we address this challenge by introducing a strategy that links ALDH2 activity to detectable metabolic incorporation of azide groups onto proteins that can be subsequently labeled with fluorophores. This approach, conditional metabolic labeling for enzymic activity detection (cMLEAD), leverages ALDH2's catalytic oxidation of azido-tagged acetaldehyde to azidoacetate, which is then funneled through the cellular metabolic machinery to produce azido-acetyl-CoA and subsequently azido-acetylated proteins.[25,26] As a result, azidoacetaldehyde-derived protein azido-acetylation can serve as downstream proxy for ALDH2 activity (Fig. 1C). By coupling enzyme-specific substrate conversion with the metabolic labeling framework, cMLEAD enables the live-cell monitoring of enzyme activities that tolerate only minimal substrate modifications. We validated this concept using azido-tagged acetaldehyde and fluorescent click chemistry to monitor protein labeling. This assay reliably measured ALDH2 activity, as confirmed by genetic modulation of ALDH2 expression and pharmacological perturbations using specific activators and inhibitors. Furthermore, cMLEAD revealed decreased cellular ALDH2 activity under glucose deprivation and senescence, with direct inhibition by $H_2O_2$ likely contributing in part. We also developed a screening platform using cMLEAD and identified a candidate ALDH2 activator. These findings highlight the utility of cMLEAD for mechanistic investigation and therapeutic discovery. While this study focuses on ALDH2, the conceptual framework of cMLEAD may be extended to other enzymes, provided that their catalytic products feed into metabolic incorporation.

## Results and discussion

### Developing the cMLEAD strategy for imaging ALDH2 activity in live cells

Alcohol-derived acetaldehyde is metabolized into acetate by ALDH2, which subsequently contributes to protein

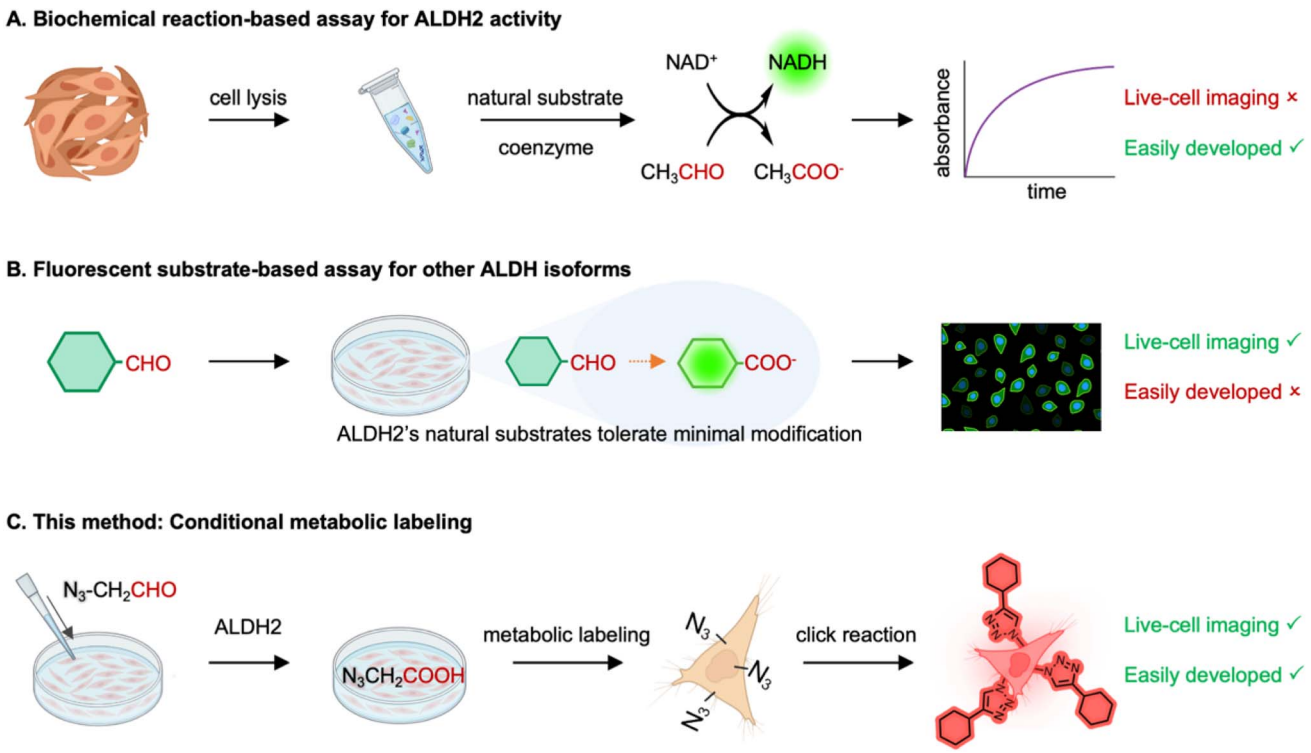


Fig. 1 (A) General procedures for the traditional biochemical reaction-based assay to measure ALDH2 activity. (B) Fluorescent probe-based assay holds promise to image ALDH2 activity in live cells, while probe development is challenging. (C) cMLEAD interrogates ALDH2 activity in live cells by integrating ALDH2-dependent oxidation of azidoacetaldehyde and metabolic labeling.

Open Access Article. Published on 20 August 2025. Downloaded on 11/7/2025 7:42:28 PM.
This article is licensed under a Creative Commons Attribution-NonCommercial 3.0 Unported Licence.

acetylation.[26–29] Capitalizing on this metabolic linkage, we hypothesized that ALDH2 activity could be indirectly measured by detecting acetylation derived from tagged acetaldehyde. Given the small size of the azido group, its established utility in biomolecule labeling, and the high efficiency of copper-catalyzed azide–alkyne cycloaddition (CuAAC),[30–32] we employed azido-tagged acetaldehyde ($AAN_3$) as the surrogate substrate. We envisioned that $AAN_3$ would be oxidized by ALDH2 to azidoacetate, subsequently converted to azido-acetyl-CoA, and incorporated into protein acetylation. The resulting azido-labeled proteins could then be visualized through CuAAC using a fluorescent alkyne, with the signal intensity proportional to cellular ALDH2 activity (Fig. 2A).

The feasibility of this approach hinges on fulfilling the following four key criteria. First, $AAN_3$ must serve as an ALDH2 substrate. Previous studies support the feasibility of $AAN_3$ serving as a substrate for ALDH2 because larger aldehydes have been shown to be processed as substrates of this enzyme.[23,24] To evaluate this, we measured kinetic parameters of recombinant human ALDH2 to $AAN_3$ *versus* the native substrate acetaldehyde (AA), by quantifying $NAD^+$ to NADH conversion. Both substrates were successfully converted by ALDH2, confirming $AAN_3$'s compatibility. However, $AAN_3$ (80 μM) exhibited almost 40-fold higher $K_m$ than AA (1.8 μM) (Fig. 2B), underscoring ALDH2's limited tolerance for substrate modifications and supporting the need for a metabolic labeling-based detection method. Fortunately, the catalytic efficiency ($K_{cat}/K_m$) towards $AAN_3$ (1.6 $min^{-1}$ $\mu M^{-1}$) was only 10-fold compromised compared to AA (17 $min^{-1}$ $\mu M^{-1}$), warranting further study.

Second, $AAN_3$ should not significantly alter endogenous protein acetylation levels, thereby ensuring an accurate readout of ALDH2 activity. To assess this, we examined cellular lysine

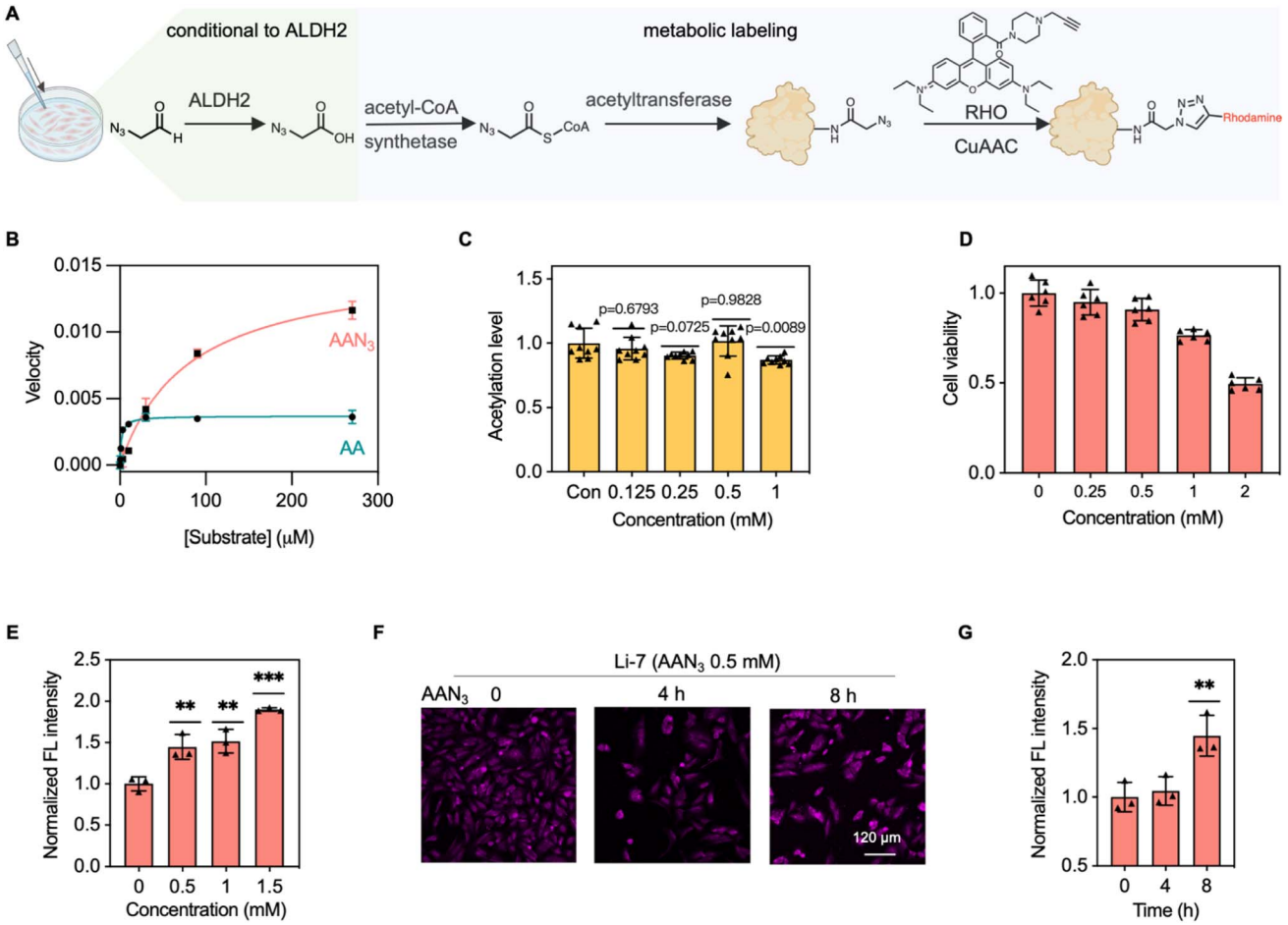


Fig. 2 Verifying cMLEAD strategy for imaging ALDH2 activity. (A) The biochemical mechanism of the strategy. (B) Enzymatic kinetics of ALDH2 to $AAN_3$ in comparison to acetaldehyde (AA). $K_m$ was 1.4–2.4 μM for AA and 62.7–105 μM for $AAN_3$ (95% confidence interval). (C) $AAN_3$ has little effect on cellular acetylation levels. HepG2 cells were treated with $AAN_3$ for 8 h and immunoassayed with a pan-acetyl lysine rabbit monoclonal antibody. The data shown were the normalized immunofluorescence intensity. (D) Cytotoxicity test of $AAN_3$. Li-7 cells were incubated with $AAN_3$ for 8 h. The viability was measured with the MTT assay, and data were normalized to the control group. (E) Quantified fluorescent intensity in Li-7 cells pretreated with various doses of $AAN_3$ for 8 h, fixed, and then subjected to classical click labeling conditions with 5 μM RHO for 1 h. (F) Representative confocal fluorescence images of Li-7 cells after being incubated with $AAN_3$ for various durations, fixed with 4 °C methanol for 10 min, and then subjected to classical click labeling conditions with 5 μM RHO for 1 h in the presence of 0.5 mM $CuSO_4$, 1.0 mM TCEP, and 100 μM TBTA. Scale bar = 120 μm. (G) Quantified fluorescent intensity in (F). Data were normalized to the $AAN_3$ (0 h) group. All experiments were carried out with 3 biologically independent replicates. *P* values were analyzed by one-way ANOVA, 95% confidence interval. Error bars represent S.D. ($n = 3$). $^{**}p < 0.01$, $^{***}p < 0.001$.

 © 2025 The Author(s). Published by the Royal Society of Chemistry

Open Access Article. Published on 20 August 2025. Downloaded on 11/7/2025 7:42:28 PM. This article is licensed under a Creative Commons Attribution-NonCommercial 3.0 Unported Licence.

acetylation using a pan-acetyl lysine antibody. At concentrations up to 0.5 mM, $AAN_3$ had a negligible impact on global acetylation levels under the assay conditions; however, 1.0 mM $AAN_3$ led to a noticeable decrease (Fig. 2C and S1), suggesting that working concentrations under 0.5 mM may be tolerable.

Third, $AAN_3$ should exhibit low cytotoxicity. An MTT assay in Li-7 human liver cancer cells revealed no significant toxicity at concentrations up to 0.5 mM after 8 hours of incubation. In contrast, concentrations above 1.0 mM resulted in a marked decrease in cell viability (Fig. 2D), reinforcing 0.5 mM $AAN_3$ as a physiologically compatible dose.

Fourth, the $AAN_3$-derived azidoacetate must be recognized by endogenous acetyl-CoA synthetases and further processed by acetyltransferases to generate azido-labeled acylated proteins. To validate this, Li-7 cells pretreated with $AAN_3$ were subjected to a classical CuAAC condition,[33] labelled with an alkyne-Rhodamine (RHO) synthesized according to literature procedures.[34] Confocal imaging showed an $AAN_3$ dose- (Fig. 2E and S2) and incubation time-dependent increase in cellular fluorescence (Fig. 2F and G), with $AAN_3$ at 0.5 mM and an incubation time of 8 h giving a statistically significant increase of cellular RHO fluorescence. This suggests the proposed metabolic incorporation of the azido group into proteins as shown in Fig. 2A. To exclude the possibility of direct covalent crosslinking of $AAN_3$ with proteins or nucleic acids, we treated the samples with methoxyamine prior to CuAAC, a procedure generally employed to release aldehyde-induced crosslinking in chemoproteomics.[35] No significant difference in cellular fluorescence intensity was observed between the samples with and without methoxyamine treatment (Fig. S3). This suggests minimal interference from aldehyde-induced conjugation effects, likely eliminated by the stringent CuAAC washing steps. Notably, background fluorescence was detected in cells without $AAN_3$ pretreatment, indicating nonspecific binding of the RHO fluorophore. This nonspecific binding is also found in a commercial alkynyl Rhodamine (Fig. S4). Together, these results confirm that $AAN_3$-derived metabolites are successfully incorporated into protein acetylation, providing a robust foundation for imaging ALDH2 activity using the cMLEAD strategy.

### Optimizing CuAAC conditions to improve imaging sensitivity

After confirming the feasibility of cMLEAD for measuring ALDH2 activity, we optimized the experimental conditions to enhance detection sensitivity. Initial tests, where cells were incubated with $AAN_3$ (0.5 mM) for 8 h followed by classical CuAAC reaction conditions, yielded only a modest 1.5-fold increase in fluorescence intensity compared to the vehicle group (Fig. 2G). This limited sensitivity was attributed to two primary factors, the low proportion of protein acetylation by acetyl-CoA, which also functions as an essential energy precursor, and the low efficiency of CuAAC under complex cellular environments. To improve CuAAC efficiency and imaging contrast, we systematically optimized the reaction conditions.

In CuAAC, a chelating ligand is necessary to protect the copper cation from generating excessive reactive oxygen species and to minimize side reactions.[36] The catalytic Cu(I) species is generated by reducing Cu(II) *in situ* to catalyze the cycloaddition between an azide and an alkyne.[37] According to this mechanism, both the reducing agent, Cu(II) dose, and the chelating ligand should be critical to determine the reaction efficiency. By systematic optimization on these three parameters (Fig. S5–S7), the final CuAAC reaction conditions were set at 0.5 mM $CuSO_4$, 2.5 mM Vc, and 600 μM THPTA, resulting in a 35-fold increase in cellular fluorescence intensity compared to the initial conditions. Further optimization on the click reaction time and RHO concentration revealed 2.5 μM RHO and a 60-min reaction time as optimal (Fig. S8 and S9).

### Validating the cMLEAD strategy for ALDH2 activity

To rigorously validate cMLEAD for faithfully reporting ALDH2 activity, we modulated ALDH2 activity in HepG2 cells through genetic and pharmacological means. Lentiviral vector infection carrying either the ALDH2 gene or its small interfering RNAs (siRNAs) generated HepG2 cells with ALDH2 overexpression or knockdown. Western blot analysis confirmed the expected upregulation and downregulation of ALDH2 protein levels (Fig. S10). Consistently, cMLEAD staining showed a pronounced increase in fluorescence intensity in ALDH2-overexpressing cells, whereas ALDH2-knockdown cells exhibited a near-complete loss of signal (Fig. 3A and B), indicating that the observed fluorescence in the cMLEAD assay is tightly correlated with ALDH2 activity.

To further validate the reliability of the strategy, we pharmacologically modulated ALDH2 activity using well-characterized small molecules. HepG2 cells were treated with Alda-1, a known ALDH2 activator,[17] or dyclonine, an ALDH2 inhibitor,[38] prior to cMLEAD labeling. Alda-1 induced a dose-dependent increase in cMLEAD fluorescence intensity, with an $EC_{50}$ of 11 μM (Fig. 3D, E and S11), consistent with reported values.[17] Conversely, dyclonine treatment caused a dose-dependent decrease in fluorescence (Fig. 3D, F and S12). While the $IC_{50}$ of dyclonine could not be accurately determined due to cytotoxicity at higher concentrations, the trend supports the dependence of cMLEAD signal on ALDH2 activity. Notably, neither Alda-1 nor dyclonine altered the expression levels of ALDH2 (Fig. S13), indicating that the observed fluorescence changes were due to functional modulation of enzymatic activity rather than changes in enzyme abundance. To check if the pharmacological treatments affected protein acetylation, we performed immunofluorescence staining with the pan acetyl lysine monoclonal antibody. No significant global changes were observed across treatment groups under the assay condition (Fig. S14), supporting ALDH2-dependence of the cMLEAD readout. In addition, ALDH2 activity was independently evaluated using a conventional NADH-based assay after cell lysis, and the resulting trends mirrored those seen with cMLEAD labeling (Fig. 3C), reinforcing the assay's reliability. Collectively, these results establish cMLEAD as an ALDH2-dependent live-cell imaging platform for quantifying its activity with desirable sensitivity. The consistency across genetic and pharmacological manipulations underscores its utility not only for biological

Open Access Article. Published on 20 August 2025. Downloaded on 11/7/2025 7:42:28 PM.
This article is licensed under a Creative Commons Attribution-NonCommercial 3.0 Unported Licence.

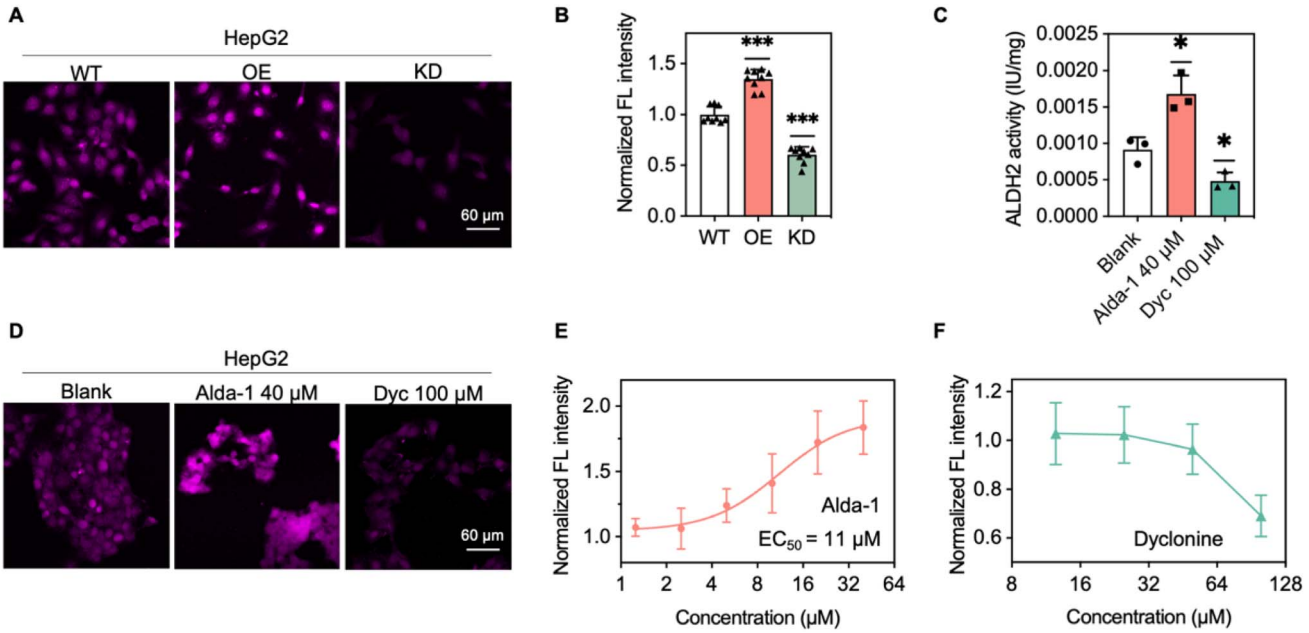


Fig. 3 Verifying the cMLEAD strategy for ALDH2 activity. (A) Confocal fluorescence images of HepG2 cells first genetically overexpressing (OE) or knocking down (KD) ALDH2 expression levels and then subjected to the optimized cMLEAD labeling conditions. (B) The quantified cellular fluorescent intensity in (A). Data were normalized to the wild type (WT) group. (C) ALDH2 activity in HepG2 cell lysate as measured by the standard NADH assay after the cells were pretreated with ALDH2 agonist Alda-1 or inhibitor Dyclonine (Dyc) for 12 h. (D) Representative confocal fluorescence images of HepG2 cells pretreated with Alda-1 or Dyc for 12 h and then subjected to the optimized cMLEAD labeling conditions. Representative images are shown from $n = 3$ independent experiments. Scale bar = 60 μm. (E and F) The quantified cellular fluorescent intensity *versus* Alda-1 or Dyclonine concentrations. Data were normalized to the blank group. An agonist *vs.* response nonlinear fit was used for Alda-1 dose effect analysis and the half effective concentration was 7.4–118 mM (95% confidence interval) or 11 μM (best fit value). All error bars represent S.D. ($n = 3$). *P* values were analyzed by one-way ANOVA. $^{**}p < 0.01$, $^{***}p < 0.001$.

investigations but also for screening small-molecule modulators of ALDH2 in cellular settings.

### Subcellular localization of $AAN_3$-derived protein acetylation

To further validate the mechanism underlying the cMLEAD strategy for measuring ALDH2 activity by measuring $AAN_3$-derived protein acetylation, we performed colocalization experiments to investigate the spatial relationship between the RHO fluorescence signal from cMLEAD and proteins typically subject to acetylation. For this purpose, we selected α-tubulin as a representative cytoplasmic protein and histone H3 as a representative nuclear protein. Following cMLEAD labeling, cells were subsequently stained with an *anti*-α-tubulin antibody, an *anti*-acetyl-histone H3 (Lys14) antibody, and DAPI. These staining procedures were designed to spot α-tubulin, acetylated histone H3 (Lys14), and the nucleus, respectively.

Multiplex imaging revealed that the RHO signal predominantly localized to the nucleus (Fig. 4A). This result suggests that acetate-derived protein acylation mainly takes place in the nucleus, consistent with the dominant nuclear distribution of acetate-dependent acetyl-CoA synthetase 2 (ACSS2), the primary enzyme generating acetyl-CoA from acetate for histone acetylation.[25,39,40] Noteworthy, the Pearson's correlation coefficient between the RHO signal and acetylated histone H3 signal was 0.62 (Fig. 4B and C), suggesting that ALDH2-generated azidoacetate works as a mimic of native acetate to acylate histones. Additionally, moderate colocalization was observed between the RHO and α-tubulin signals (Pearson's coefficient = 0.63) (Fig. 4D and E), consistent with previous findings that chronic ethanol exposure enhances tubulin acetylation.[41] This result provides the first direct evidence that upregulated acetylation of α-tubulin is at least partially derived from the carbon source provided by ingested alcohol. All these results confirm the mechanism of cMLEAD, which integrates ALDH2's catalytic conversion of aldehydes to acetate with the cellular metabolic machinery of utilizing acetate for protein acetylation. This highlights the strategy's unique capability to exploit native cellular processes for interrogating enzyme activity.

### Applying cMLEAD to interrogate ALDH2 activity upon various stress conditions

ALDH2 is implicated in pathological processes such as cardiovascular disorders, neurodegenerative diseases, and metabolic dysregulation. However, it remains unclear how its activity is regulated under various cellular stresses. Measuring ALDH2 activity is crucial for understanding its dynamic regulation under disease-relevant stress conditions, including oxidative damage, hypoglycemia, and cellular senescence. Such insights could inform the development of ALDH2 activators to mitigate stress-induced damage and restore cellular homeostasis.

With the cMLEAD strategy established, we applied it to investigate how ALDH2 activity responds to cellular stress

 © 2025 The Author(s). Published by the Royal Society of Chemistry

Open Access Article. Published on 20 August 2025. Downloaded on 11/7/2025 7:42:28 PM.
This article is licensed under a Creative Commons Attribution-NonCommercial 3.0 Unported Licence.

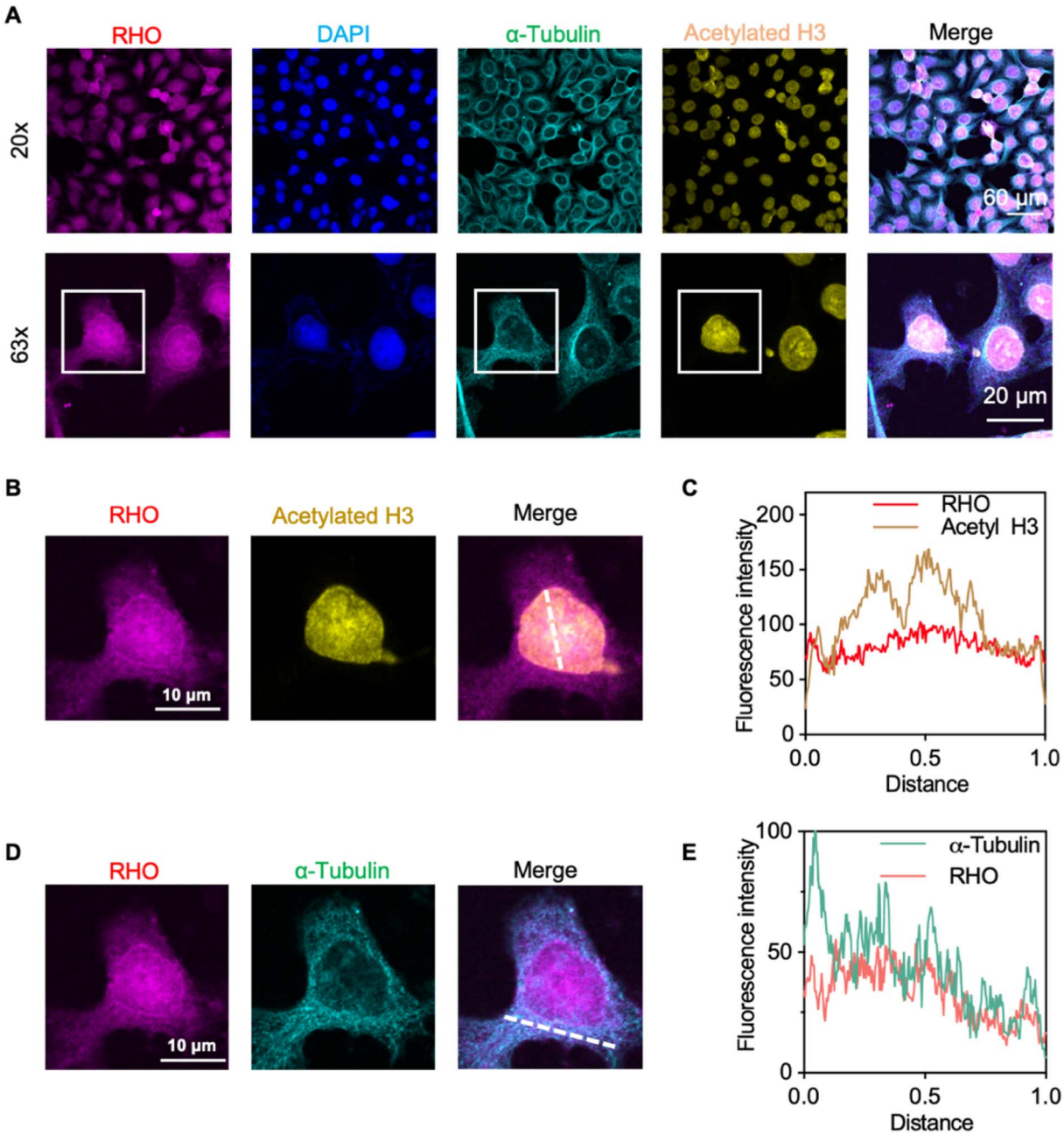


Fig. 4 Spatial localization of $AAN_3$-induced acetylation. (A) Confocal fluorescence images of HepG2 cells stained with cMLEAD (RHO, magenta), *anti*-α-tubulin (teal), *anti*-acetyl histone H3 (Lys14) (yellow), and DAPI (blue). Scale bar = 60 μm for the top panel and 20 μm for the bottom panel. (B and D) The enlarged image of the indicated cell in (A) with the indicated fluorescence signals. (C and E) The quantified co-localization analysis in (B) or (D) shown by the white dashed line. Pearson correlation coefficient = 0.62 (C) and 0.63 (E).

conditions. We focused on bleomycin-induced senescence and glucose deprivation-induced metabolic stress in HepG2 cells.[42,43] Cells treated with increasing doses of bleomycin for 48 h exhibited a dose-dependent senescent phenotype, confirmed by β-galactosidase (β-Gal) staining (Fig. 5A and C). cMLEAD labeling revealed a clear inverse correlation between RHO fluorescence intensity and bleomycin concentration (Fig. 5A and D), indicating a progressive reduction in ALDH2 activity during senescence. To validate that this observation was not confounded by global changes in protein acetylation, we performed immunofluorescence staining using the pan-acetyl lysine antibody. No significant difference in protein acetylation levels was observed across treatment groups under the assay conditions (Fig. S15), supporting the ALDH2 activity-dependence of the cMLEAD signal. Moreover, western blot analysis revealed no significant change in ALDH2 protein expression level upon bleomycin exposure (40 μM, 48 h) (Fig. S13). NADH-based ALDH2 assay in cell lysates confirmed the decreasing trend in enzymatic activity, in agreement with the cMLEAD results (Fig. 5E). These findings align with previous

Open Access Article. Published on 20 August 2025. Downloaded on 11/7/2025 7:42:28 PM.
This article is licensed under a Creative Commons Attribution-NonCommercial 3.0 Unported Licence.

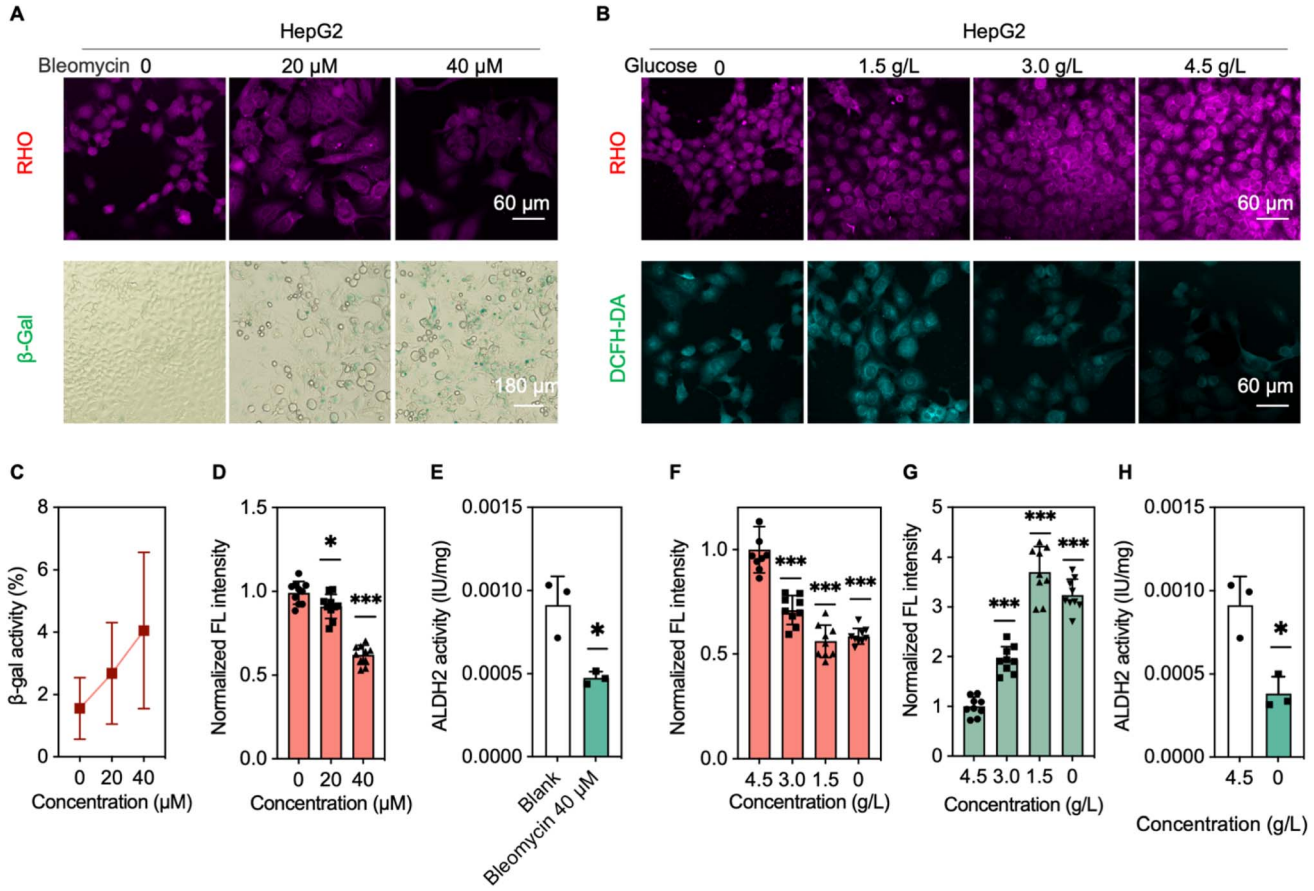


Fig. 5 Interrogating ALDH2 activity under various cellular stress. (A) Confocal fluorescence and inverted microscope images of bleomycin-induced senescent HepG2 cells. Cells were treated with bleomycin for 48 h and then either stained with a β-Gal kit to verify senescence or were subjected to cMLEAD labeling. Representative images are shown from $n = 3$ independent experiments. Scale bar = 60 μm. (B) Confocal fluorescence images of HepG2 cells first stimulated under low-glucose conditions (8 h) and then either subjected to cMLEAD labeling or DCFH-DA labeling. Representative images are shown from $n = 3$ independent experiments. Scale bar = 60 μm. (C) The quantified β-Gal staining results in A. Error bars represent S.D. ($n = 10$). (D) The quantified RHO fluorescence in A. Data were normalized to the vehicle treatment group. Error bars represent S.D. ($n = 9$). $P$ values were analyzed by one-way ANOVA, 95% Confidence interval. $^{*}p < 0.05$, $^{***}p < 0.001$. (E) ALDH2 activity as measured by the standard NADH assay in cell lysate after the indicated treatment. Error bars represent S.D. ($n = 3$). (F) The quantified cellular RHO labeling intensity in (B). Data were normalized to the glucose 4.5 g $L^{-1}$ group. (G) The quantified cellular DCFH-DA labeling intensity in (B). Data were normalized to the glucose 4.5 g $L^{-1}$ group. (H) ALDH2 activity as measured by the standard NADH assay in cell lysate after the indicated treatment. Error bars represent S.D. ($n = 3$). $P$ values were analyzed by one-way ANOVA, 95% Confidence interval. $^{**}p < 0.01$, $^{***}p < 0.001$.

reports linking reduced or dysfunctional ALDH2 activity to aging-related pathologies,[44] and further highlight the utility of cMLEAD for monitoring stress-induced changes in enzyme function in live cells.

Glucose deprivation similarly led to a reduction in ALDH2 activity in HepG2 cells, as revealed by cMLEAD fluorescence imaging (Fig. 5B and F). Importantly, western blot analysis showed that ALDH2 protein expression remained largely unchanged under low-glucose conditions (0 g $L^{-1}$, 8 h) (Fig. S13), indicating that the observed decrease in activity is not due to altered expression. Given the well-established link between glucose deprivation and oxidative stress, we next assessed intracellular reactive oxygen species (ROS) levels using the 2′,7′-dichlorodihydrofluorescein diacetate (DCFH-DA) probe. A marked increase in DCFH-DA fluorescence was detected following glucose deprivation, confirming elevated oxidative stress (Fig. 5B and G). Notably, the extent of ROS accumulation was inversely correlated with ALDH2 activity as measured by cMLEAD, suggesting that oxidative stress may impair ALDH2 enzymatic function. Protein acetylation immunostaining (Fig. S16) and NADH-based ALDH2 activity assay in cell lysates (Fig. 5H) further confirmed the selective suppression of ALDH2 activity without significant disruption of cellular protein acetylation levels. These findings reinforce the conclusion that oxidative stress compromises ALDH2 function, which is detectable by cMLEAD, consistent with previous reports linking oxidative stress to aldehyde accumulation and metabolic dysfunction.[45–47]

To shed light on the mechanism underlying the compromised ALDH2 activity under these stress conditions, we investigated the direct effects of typical oxidative stress-associated metabolites on ALDH2 enzymatic function. Specifically, we assessed the impact of hydrogen peroxide ($H_2O_2$), which accumulates during oxidative stress, using a recombinant ALDH2-

 © 2025 The Author(s). Published by the Royal Society of Chemistry

Open Access Article. Published on 20 August 2025. Downloaded on 11/7/2025 7:42:28 PM.
This article is licensed under a Creative Commons Attribution-NonCommercial 3.0 Unported Licence.

based NADH assay. $H_2O_2$ was found to inhibit ALDH2 activity in a dose-dependent manner, with $IC_{50}$ of 40 μM (Fig. S17). While the precise mechanism underlying the observed reduction in ALDH2 activity under oxidative and senescence-related stress remains to be elucidated, our results suggest that ALDH2 is functionally sensitive to redox modulation. Importantly, cMLEAD enables the detection of such dynamic enzymatic changes in live-cell contexts, providing a valuable tool for monitoring stress-induced alterations in enzyme activity.

### Screening and identifying candidate ALDH2 activators using cMLEAD

The observed decline in ALDH2 activity under oxidative stress and senescence (Fig. 5), along with its established link to

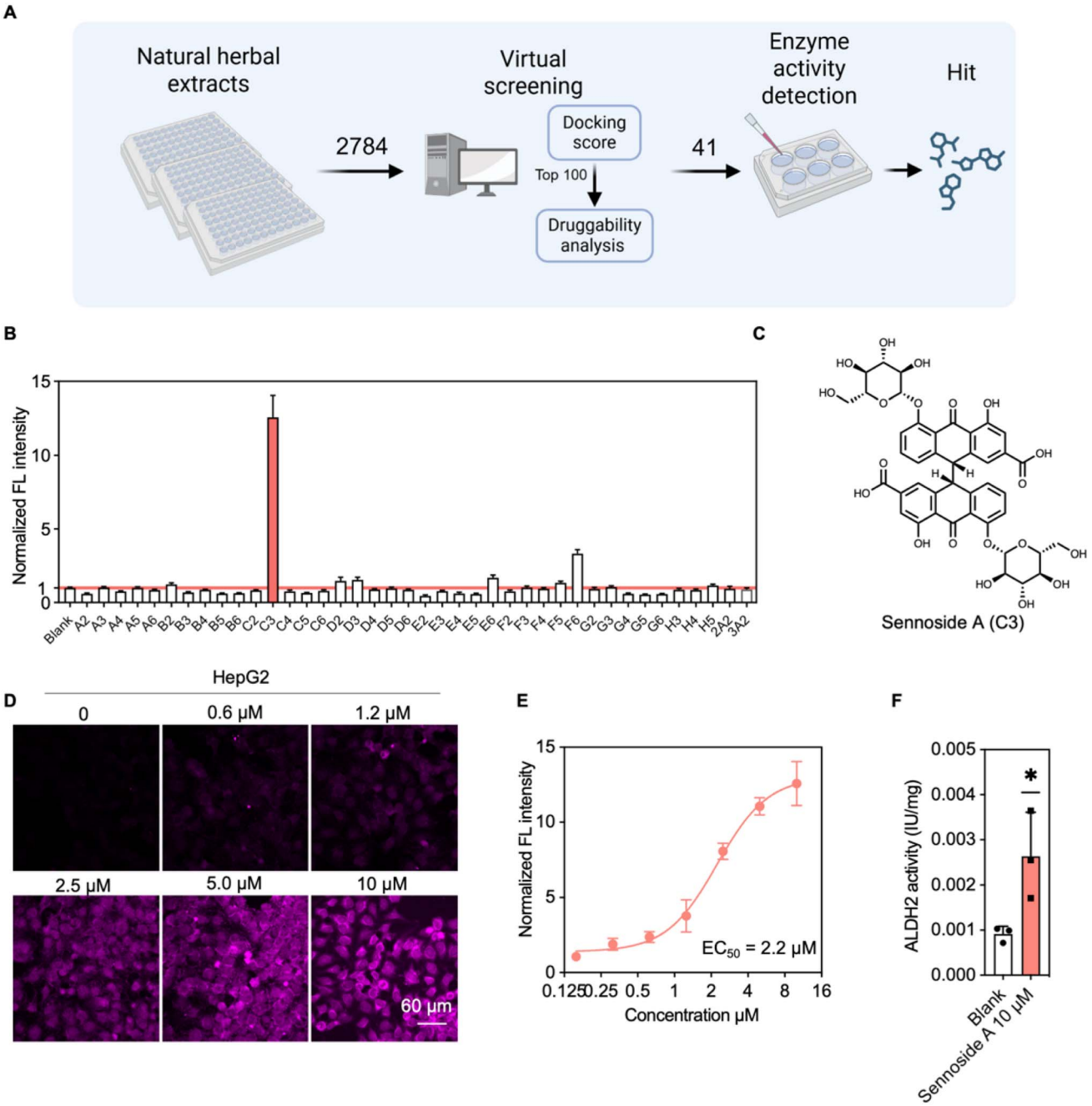


Fig. 6 Screening for candidate ALDH2 modulators with cMLEAD. (A) Screening process pattern diagram. (B) The quantified cellular fluorescence intensity after cMLEAD labeling. HepG2 cells were first treated with the indicated compound (10 μM) in Table S2 for 12 h, and then subjected to cMLEAD labeling. Data were normalized to the blank treatment group. (C) Structure of sennoside A. (D) Representative confocal fluorescence images of HepG2 cells first treated with sennoside A (12 h) and then subjected to cMLEAD staining. Scale bar = 60 μm. (E) The quantified data in D. An agonist *vs.* response nonlinear fit was used to determine the dose effect, and the half-effective concentration was determined to be 2.0–2.5 μM (95% Confidence interval). Error bars represent S.D. ($n = 3$). (F) ALDH2 activity as measured by the standard NADH assay in cell lysate after treating cells with sennoside A. Error bars represent S.D. ($n = 3$).

Open Access Article. Published on 20 August 2025. Downloaded on 11/7/2025 7:42:28 PM.
This article is licensed under a Creative Commons Attribution-NonCommercial 3.0 Unported Licence.

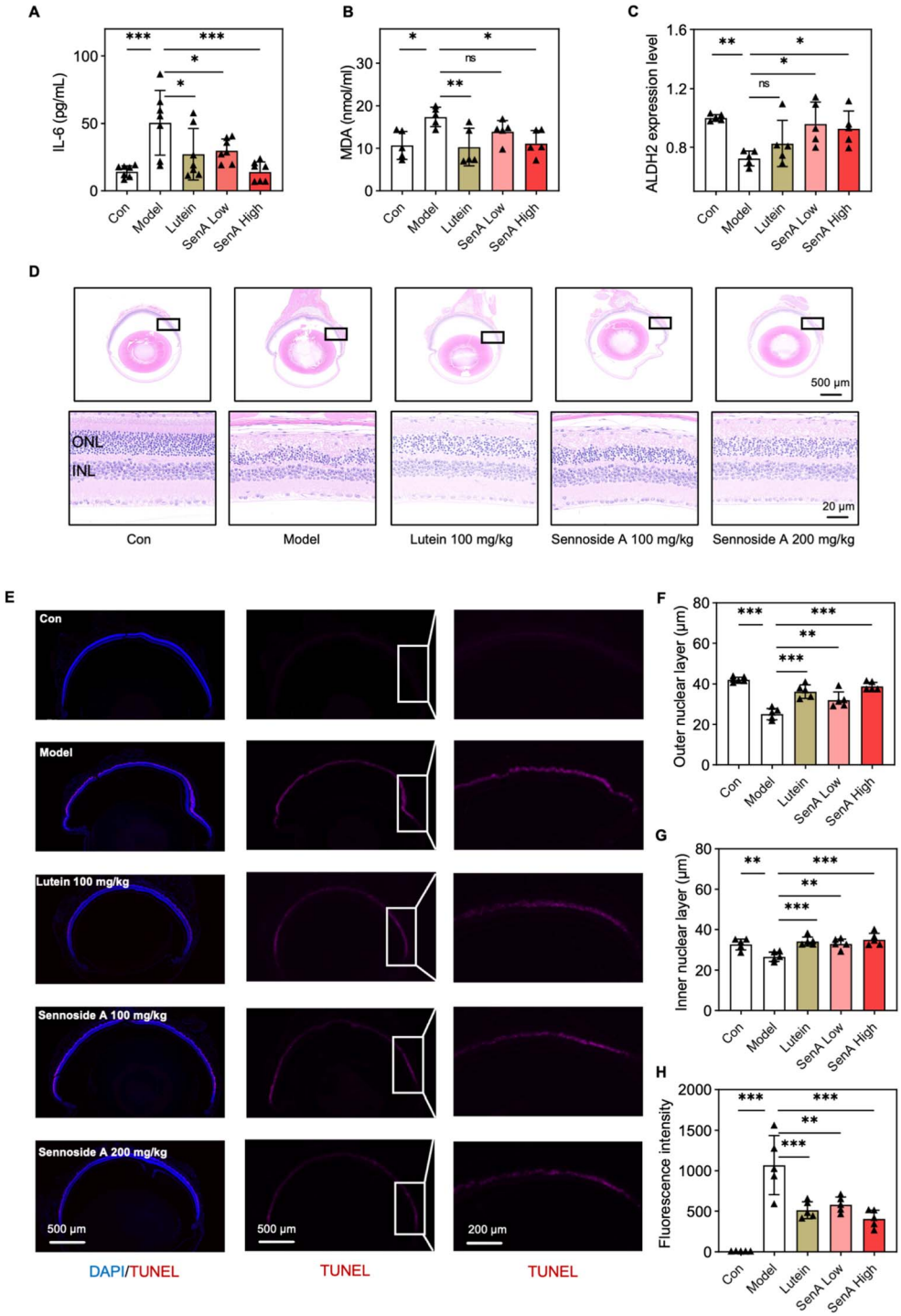


Fig. 7 Validating sennoside A's activity in a light-induced retinal degeneration mouse model. (A and B) Quantification of IL-6 levels ($n = 7$) and malondialdehyde contents ($n = 5$) in mouse plasma after the indicated drug treatment and the light-induced retinal degeneration modeling. Error bars represent S.D. $P$ values were analyzed by one-way ANOVA, 95% confidence interval. (C) Quantified ALDH2 levels as measured by immunofluorescence in mouse retinal subjected to the drug treatment and modeling. (D) Mouse retinal H&E staining images. (E) TUNEL staining of apoptotic cells in the mouse retina by fluorescence microscope. DAPI (blue), TUNEL (red). Representative images are shown from $n = 5$ independent experiments. (F and G) The quantified data on mouse retinal outer nuclear layer and inner nuclear layer after the indicated drug treatment in (D). Three points were chosen from every eye retinal after H&E staining and the thicknesses of the respective layers were measured with the Case viewer (CV) Software (Servicebio Company). The average of the three data points was calculated as the final thicknesses of every eye retinal inner nuclear layer (INL) or outer nuclear layer (ONL). $P$ values were analyzed by one-way ANOVA, 95% Confidence interval. Error bars represent S.D. ($n = 5$). (H) The quantified data of TUNEL fluorescence intensity in (E). Signal intensity was normalized to the control group. Error bars represent S.D. ($n = 5$). $*p < 0.05$, $**p < 0.01$, $***p < 0.001$.

 © 2025 The Author(s). Published by the Royal Society of Chemistry

Open Access Article. Published on 20 August 2025. Downloaded on 11/7/2025 7:42:28 PM.
This article is licensed under a Creative Commons Attribution-NonCommercial 3.0 Unported Licence.

aging,[44] underscores the therapeutic potential of ALDH2 activation for treating aging-related diseases. We observed that cMLEAD sensitively captured Alda-1 mediated activation of ALDH2 in live cells (Fig. 3E), encouraging us to explore its feasibility to screen for ALDH2 activators. Actually, purified recombinant ALDH2 gradually loses activity at low concentrations (Fig. S18). Thus, cellular screening not only maintains enzyme stability but also identifies molecules that enhance activity either directly through allosteric activation or indirectly by increasing cofactors or modulating upstream/downstream events.

Initially, an *in silico* docking-based screening was performed on a natural compound library of 2784 structures to prioritize those with the most promising binding to ALDH2 (Table S1). The top 100 candidates were then evaluated using ADMETlab 2.0 to filter out those with unfavorable pharmacokinetic properties,[48] resulting in 41 promising structures (Table S2). HepG2 cells were incubated with these compounds, followed by cMLEAD labeling (Fig. 6A). Cellular fluorescence was used as a readout of ALDH2 activity (Fig. S19). Setting the vehicle-treated group as the baseline (Fig. 6B), we identified three activators and three inhibitors (Fig. S20–S25). Among these, sennoside A exhibited the most robust activation (Fig. 6C), with cellular fluorescence intensity 10-fold higher than the vehicle group. Further evaluation with cMLEAD determined an $EC_{50}$ of 2.2 μM for sennoside A (Fig. 6D, E and S20). Moreover, NADH-based ALDH2 activity in cell lysates after sennoside A-pretreatment also verified its activating effect (Fig. 6F). We also confirmed that sennoside A didn't affect the ALDH2's expression levels (Fig. S13), nor did it affect cellular acetylation levels under the assay conditions (Fig. S14). These findings suggest cMLEAD's applicability for screening, and also propose sennoside A as a candidate ALDH2 activator with the exact mode of action to be explored.

### Sennoside A protects against light-induced retinal degeneration in BALB/c mice

Previous studies have demonstrated that ALDH2 can alleviate retinal damage caused by oxidative stress.[49] To evaluate the activity of sennoside A *in vivo*, we employed a light-induced retinal degeneration model in mice. Animals were randomly divided into five groups: control (no light exposure, treated with 5% sodium carboxyl methyl cellulose), model (light exposure, treated with 5% sodium carboxyl methyl cellulose), low-dose sennoside A (light exposure, 100 mg per kg sennoside A), high-dose sennoside A (light exposure, 200 mg per kg sennoside A), and lutein (light exposure, 100 mg per kg lutein as a positive control). Compounds were administered intragastrically for 10 consecutive days. During the last three days of the administration, all groups except the control were first exposed to dark for 36 h, then treated with atropine ophthalmic gel to both eyes, and lastly exposed to 8500–10000 Lux light for 24 h.

A series of tests assessed the protective effects of sennoside A. Elevated plasma interleukin-6 (IL-6) levels (Fig. 7A) and malondialdehyde (MDA) levels (Fig. 7B) in the model group confirmed significant inflammation and oxidative stress induced by light exposure. Notably, high-dose sennoside A markedly alleviated these effects, comparable to the positive control Lutein, suggesting its protective potential. Although the total antioxidant capacity (T-AOC) assay didn't reach statistical significance, a dose-dependent protective trend was observed (Fig. S26). Since sennoside A is known to exhibit multiple cellular activities, including antioxidant and anti-inflammatory effects,[50,51] we interrogated the involvement of ALDH2 in the observed protective effects. Immunofluorescence staining revealed increased ALDH2 expression in retinal tissues from sennoside A-treated group relative to the model group (Fig. 7C and S27). While short-term sennoside A treatment in HepG2 cells (12 h) did not result in a significant change in ALDH2 protein expression (Fig. S13), chronic administration *in vivo* (daily for 10 days) was associated with an upward trend in ALDH2 levels. This observation raises the possibility of a positive feedback mechanism, whereby prolonged ALDH2 activation by sennoside A may reduce oxidative stress and inflammation, which in turn could stabilize ALDH2 and reduce its degradation. However, further investigation is needed to elucidate the underlying regulatory pathways.

Histopathological evaluation using H&E staining revealed light-induced retinal damage in the model group, characterized by reduced thickness and structural looseness of the outer and inner nuclear layers (Fig. 7D). Both low- and high-dose sennoside A mitigated this damage, preserving retinal morphology and reducing the thinning of the nuclear layers (Fig. 7F and G). TUNEL staining further confirmed retinal cell apoptosis caused by light exposure, indicated by increased red fluorescence in the model group (Fig. 7E). Sennoside A treatment at both doses significantly reduced apoptosis, with effects comparable to Lutein (Fig. 7H). These results validate the protective effects of sennoside A in mitigating inflammation, oxidative stress, and apoptosis in this light-induced retinal degeneration model. Since sennoside A has been verified to boost cellular ALDH2 activity (Fig. 6E and F), this study underscores the potential of the cMLEAD strategy for identifying candidate ALDH2 activators.

## Conclusion

In this study, we developed and rigorously validated the cMLEAD strategy, a metabolically-linked enzymatic activity detection method, for imaging ALDH2 activity in live cells. Integrating azido-tagged acetaldehyde into the native acetylation pathway, cMLEAD enables context-aware visualization of ALDH2 activity in live cells with desirable sensitivity. This strategy addresses the limitations of traditional biochemical assays that lack cellular context and offers a solution for interrogating the activity of enzymes in live cells that tolerate only minimal substrate modifications. cMLEAD exhibited desirable specificity and robustness across a range of conditions. Genetic overexpression and knockdown, as well as pharmacological activation and inhibition, consistently validated the assay's reliability. Application of cMLEAD to stress models such as bleomycin-induced senescence and glucose deprivation revealed that ALDH2 activity is susceptible to oxidative stress,

Open Access Article. Published on 20 August 2025. Downloaded on 11/7/2025 7:42:28 PM.
This article is licensed under a Creative Commons Attribution-NonCommercial 3.0 Unported Licence.

providing new insights into its regulation under pathological conditions. These findings highlight ALDH2's vulnerability in aging and metabolic disorders and underscore the relevance of cMLEAD in mechanistic studies. cMLEAD also proved valuable as a high-content screening platform. Using this strategy, we identified sennoside A as a potential ALDH2 activator with protective efficacy against light-induced retinal degeneration *in vivo*. This illustrates cMLEAD's translational potential in therapeutic discovery and target validation. Beyond ALDH2, cMLEAD provides a broadly applicable framework for studying enzymes with metabolically converted or unstable substrates, as long as their catalytic products feed into pathways that result in detectable metabolic incorporations. Its adaptability and physiological relevance position it as a powerful tool for enzyme activity mapping, stress biology research, and drug discovery in complex biological systems.

Nonetheless, several limitations of the cMLEAD strategy should be acknowledged. First, cMLEAD provides an indirect readout of enzyme activity that depends not only on ALDH2-mediated transformation but also on subsequent metabolic incorporation steps. As such, appropriate controls and, when possible, orthogonal validation methods are necessary to confirm enzymatic specificity. Second, the assay exhibits a relatively high background signal, which may limit sensitivity. Further optimization, such as reducing nonspecific interactions with the alkyne-functionalized fluorophore, could improve signal-to-noise ratios. Third, while cMLEAD enabled a live-cell screening platform for identifying candidate ALDH2 modulators, additional mechanistic studies are required to validate whether these hits act through direct or indirect modulation of ALDH2 activity.

## Author contributions

X. Li and X. Fan conceived the project. W. Lv did all the cell imaging experiments. Z. Wang and C. Zhang tested the protective effect of sennoside A against light-induced retinal degeneration. J. Li checked the enzymatic kinetics of ALDH2 towards AA and $AAN_3$. T. Liu analyzed the data. T. Yang performed the NADH-based ALDH2 assay in cell lysates. W. Lv drafted the manuscript. X. Li and X. Fan revised it. All authors read and approved the final manuscript.

## Conflicts of interest

The authors declare no conflict of interest.

## Data availability

The data supporting this article have been included in the SI. All methods, SI figures, SI tables, and the ethical statement for animal procedures which were performed in accordance with the Guidelines for Care and Use of Laboratory Animals of Zhejiang University and approved by the Animal Ethics Committee of Zhejiang University. See DOI: **https://doi.org/10.1039/d5sc04198h**.

## Acknowledgements

This study was supported by grants from the Natural Science Foundation of Zhejiang province (LZ23H300001) and the National Natural Science Foundation of China (22377106). X. L. was supported by the National Program for Support of Top-notch Young Professionals (grant 2021).

## References

1 A. Saghatelian and B. F. Cravatt, *Nat. Chem. Biol.*, 2005, **1**, 130–142.
2 T. K. Harris and M. M. Keshwani, *Methods Enzymol.*, 2009, **463**, 57–71.
3 P. K. Robinson, *Essays Biochem.*, 2015, **59**, 1–41.
4 A. Baruch, D. A. Jeffery and M. Bogyo, *Trends Cell Biol.*, 2004, **14**, 29–35.
5 M. Yuan, Y. Wu, C. Zhao, Z. Chen, L. Su, H. Yang and J. Song, *Theranostics*, 2022, **12**, 1459–1485.
6 S. H. Gardner, C. J. Reinhardt and J. Chan, *Angew Chem. Int. Ed. Engl.*, 2021, **60**, 5000–5009.
7 H. Singh, K. Tiwari, R. Tiwari, S. K. Pramanik and A. Das, *Chem. Rev.*, 2019, **119**, 11718–11760.
8 X. Wu, R. Wang, N. Kwon, H. Ma and J. Yoon, *Chem. Soc. Rev.*, 2022, **51**, 450–463.
9 J. I. Scott, Q. Deng and M. Vendrell, *ACS Chem. Biol.*, 2021, **16**, 1304–1317.
10 B. S. McCullough and A. M. Barrios, *Curr. Opin. Chem. Biol.*, 2020, **57**, 34–40.
11 L. Wu, Z. Armstrong, S. P. Schröder, C. de Boer, M. Artola, J. M. Aerts, H. S. Overkleeft and G. J. Davies, *Curr. Opin. Chem. Biol.*, 2019, **53**, 25–36.
12 Y. Chen and X. Li, *Curr. Med. Chem.*, 2024, **31**, 970–994.
13 M. Yang, Y. Zhang and J. Ren, *Adv. Exp. Med. Biol.*, 2019, **1193**, 229–236.
14 J. Zhang, Y. Guo, X. Zhao, J. Pang, C. Pan, J. Wang, S. Wei, X. Yu, C. Zhang, Y. Chen, H. Yin and F. Xu, *Nat. Rev. Cardiol.*, 2023, **20**, 495–509.
15 C. H. Chen, A. U. Joshi and D. Mochly-Rosen, *Acta Neurol. Taiwan*, 2016, **25**(4), 111–123.
16 H. Zhang and L. Fu, *Acta Pharm. Sin. B*, 2021, **11**, 1400–1411.
17 C. H. Chen, G. R. Budas, E. N. Churchill, M. H. Disatnik, T. D. Hurley and D. Mochly-Rosen, *Science*, 2008, **321**, 1493–1495.
18 R. Tao, M. Liao, Y. Wang, H. Wang, Y. Tan, S. Qin, W. Wei, C. Tang, X. Liang, Y. Han and X. Li, *Anal. Chem.*, 2022, **94**, 1308–1317.
19 C. Xu, L. Zhang, S. Xu, Z. Wang, Q. Han, Y. Lv, X. Wang, X. Zhang, Q. Zhang, Y. Zhang, S. He, Q. Yuan, Y. Bian, C. Li, J. Wang, F. Xu, Y. Cao, J. Pang and Y. Chen, *Cell. Mol. Immunol.*, 2024, **21**, 510–526.
20 C. Anorma, J. Hedhli, T. E. Bearrood, N. W. Pino, S. H. Gardner, H. Inaba, P. Zhang, Y. Li, D. Feng, S. E. Dibrell, K. A. Kilian, L. W. Dobrucki, T. M. Fan and J. Chan, *ACS Cent. Sci.*, 2018, **4**, 1045–1055.
21 S. Maity, C. M. Sadlowski, J. M. George Lin, C. H. Chen, L. H. Peng, E. S. Lee, G. K. Vegesna, C. Lee, S. H. Kim,

 © 2025 The Author(s). Published by the Royal Society of Chemistry

Open Access Article. Published on 20 August 2025. Downloaded on 11/7/2025 7:42:28 PM.
This article is licensed under a Creative Commons Attribution-NonCommercial 3.0 Unported Licence.

D. Mochly-Rosen, S. Kumar and N. Murthy, *Chem. Sci.*, 2017, **8**, 7143–7151.
22 S. Perez-Miller, H. Younus, R. Vanam, C. H. Chen, D. Mochly-Rosen and T. D. Hurley, *Nat. Struct. Mol. Biol.*, 2010, **17**, 159–164.
23 A. A. Klyosov, *Biochemistry*, 1996, **35**, 4457–4467.
24 M. F. Wang, C. L. Han and S. J. Yin, *Chem. Biol. Interact.*, 2009, **178**, 36–39.
25 P. Mews, G. Donahue, A. M. Drake, V. Luczak, T. Abel and S. L. Berger, *Nature*, 2017, **546**, 381–386.
26 P. Mews, G. Egervari, R. Nativio, S. Sidoli, G. Donahue, S. I. Lombroso, D. C. Alexander, S. L. Riesche, E. A. Heller, E. J. Nestler, B. A. Garcia and S. L. Berger, *Nature*, 2019, **574**, 717–721.
27 A. I. Cederbaum, *Clin. Liver Dis.*, 2012, **16**, 667–685.
28 S. Zakhari, *Alcohol Res.*, 2013, **35**, 6–16.
29 S. C. Pandey and J. P. Bohnsack, *Cell Metab.*, 2020, **31**, 213–214.
30 N. Klöcker, F. P. Weissenboeck and A. Rentmeister, *Chem. Soc. Rev.*, 2020, **49**, 8749–8773.
31 T. W. Bumpus and J. M. Baskin, *Trends Biochem. Sci.*, 2018, **43**, 970–983.
32 H. Xiao, S. Suttapitugsakul, F. Sun and R. Wu, *Acc. Chem. Res.*, 2018, **51**, 1796–1806.
33 A. E. Speers and B. F. Cravatt, *Chem. Biol.*, 2004, **11**, 535–546.
34 N. B. Yapici, S. Mandalapu, K. M. Gibson and L. Bi, *Bioorg. Med. Chem. Lett.*, 2015, **25**, 3476–3480.
35 J. Li, J. Zhou, H. Xu, K. Tian, H. Zhu, Y. Chen, Y. Huang, G. Wang, Z. Gong, H. Qin and M. Ye, *J. Am. Chem. Soc.*, 2023, **145**, 5252–5260.
36 C. Besanceney-Webler, H. Jiang, T. Zheng, L. Feng, D. Soriano del Amo, W. Wang, L. M. Klivansky, F. L. Marlow, Y. Liu and P. Wu, *Angew Chem. Int. Ed. Engl.*, 2011, **50**, 8051–8056.
37 V. V. Rostovtsev, L. G. Green, V. V. Fokin and K. B. Sharpless, *Angew Chem. Int. Ed. Engl.*, 2002, **41**, 2596–2599.
38 M. Khanna, C. H. Chen, A. Kimble-Hill, B. Parajuli, S. Perez-Miller, S. Baskaran, J. Kim, K. Dria, V. Vasiliou, D. Mochly-Rosen and T. D. Hurley, *J. Biol. Chem.*, 2011, **286**, 43486–43494.
39 D. C. Alexander, T. Corman, M. Mendoza, A. Glass, T. Belity, R. Wu, R. R. Campbell, J. Han, A. A. Keiser, J. Winkler, M. A. Wood, T. Kim, B. A. Garcia, H. Cohen, P. Mews, G. Egervari and S. L. Berger, *Proc. Natl. Acad. Sci. U. S. A.*, 2022, **119**, e2114758119.
40 M. Mendoza, G. Egervari, S. Sidoli, G. Donahue, D. C. Alexander, P. Sen, B. A. Garcia and S. L. Berger, *Sci. Adv.*, 2022, **8**, eabj5688.
41 G. T. Kannarkat, D. J. Tuma and P. L. Tuma, *J. Hepatol.*, 2006, **44**, 963–970.
42 K. Aoshiba, T. Tsuji and A. Nagai, *Eur. Respir. J.*, 2003, **22**, 436–443.
43 H. Monyer, M. P. Goldberg and D. W. Choi, *Brain Res.*, 1989, **483**, 347–354.
44 N. N. Wu and J. Ren, *Adv. Exp. Med. Biol.*, 2019, **1193**, 237–253.
45 J. Endo, M. Sano, T. Katayama, T. Hishiki, K. Shinmura, S. Morizane, T. Matsuhashi, Y. Katsumata, Y. Zhang, H. Ito, Y. Nagahata, S. Marchitti, K. Nishimaki, A. M. Wolf, H. Nakanishi, F. Hattori, V. Vasiliou, T. Adachi, I. Ohsawa, R. Taguchi, Y. Hirabayashi, S. Ohta, M. Suematsu, S. Ogawa and K. Fukuda, *Circ. Res.*, 2009, **105**, 1118–1127.
46 S. Singh, C. Brocker, V. Koppaka, Y. Chen, B. C. Jackson, A. Matsumoto, D. C. Thompson and V. Vasiliou, *Free Radic. Biol. Med.*, 2013, **56**, 89–101.
47 A. C. Flor and S. J. Kron, *Cell Death Dis.*, 2016, **7**, e2366.
48 G. Xiong, Z. Wu, J. Yi, L. Fu, Z. Yang, C. Hsieh, M. Yin, X. Zeng, C. Wu, A. Lu, X. Chen, T. Hou and D. Cao, *Nucleic Acids Res.*, 2021, **49**, W5–W14.
49 P. Long, M. He, W. Yan, W. Chen, D. Wei, S. Wang, Z. Zhang, W. Ge and T. Chen, *Aging (Albany NY)*, 2020, **13**, 2750–2767.
50 M. M. Alshehri, C. Quispe, J. Herrera-Bravo, J. Sharifi-Rad, S. Tutuncu, E. F. Aydar, C. Topkaya, Z. Mertdinc, B. Ozcelik, M. Aital, N. V. A. Kumar, N. Lapava, J. Rajkovic, A. Ertani, S. Nicola, P. Semwal, S. Painuli, C. González-Contreras, M. Martorell, M. Butnariu, I. C. Bagiu, R. V. Bagiu, M. D. Barbhai, M. Kumar, S. D. Daștan, D. Calina and W. C. Cho, *Oxid. Med. Cell. Longev.*, 2022, **2022**, 6025900.
51 H. Zhu, H. Zhao, S. Xu, Y. Zhang, Y. Ding, J. Li, C. Huang and T. Ma, *Pharmacol. Res.*, 2021, **174**, 105926.